# High angular resolution diffusion imaging methods: a diffusion phantom study

Ezequiel Farrher[1], Tony Stöcker[1], Farida Grinberg[1], and N. Jon Shah[1,2]

[1]*Institute of Neuroscience and Medicine - 4, Forschungszentrum Juelich, Juelich, Germany,* [2]*JARA - Faculty of Medicine, RWTH Aachen University, Aachen, Germany*

## Introduction

During the last two decades the diffusion tensor imaging (DTI) technique has become a prime tool in the investigation of brain structure and connectivity. However, a well-known disadvantage of DTI is related to its inability to model complex fibre structures such as crossing or diverging fibres. Several methods based on high angular resolution diffusion imaging (HARDI) have been proposed to circumvent this problem. In order to enable a quantitative validation of the proposed models to elucidate tissue orientation, it is necessary to have artificial systems with well-known structure and physical properties. We demonstrate here the application of a multi-section diffusion phantom [1] in the investigation of the performance of two models for HARDI data analysis, i.e. the Q-ball Imaging (QBI) [2] and the constrained spherical deconvolution (CSD) [3] methods. Both approaches are compared in different fibre configurations, fibre densities and SNRs.

## Materials and methods

The phantom was built with polyethylene fibres (Dyneema® DTX 70) of 16 μm diameter [1]. Both sides of the phantom, Fig. 1, exhibit a region in which fibres cross at 90º and a region in which fibres are parallel. The fibre density, *f*, is constant on side 1 but is spatially dependent on side 2. The whole setup was immersed in a cylindrical container filled with distilled water. MRI experiments were carried out in a whole-body 3T Siemens Trio scanner (Siemens Medical Systems, Erlangen, Germany). A spin-echo EPI pulse sequence was applied with parameters: TR/TE = 2300/109 ms; voxel size, 2×2×2 $mm^3$; 16 averages; 64 gradient directions; *b*-values, 0 and 1000 $smm^{-2}$. The normalized fibre orientation distribution (FOD) in the case of CSD and the orientation density function (ODF) in the case of QBI analysis were obtained using the toolbox ExploreDTI [4]. Results from both methods were generated using spherical-harmonic order up to $l_{max}$ = 8. SNR was estimated by taking the ratio of the signal from different regions of interest (ROI) in the non-diffusion weighted image to the standard deviation of the background noise. The discrepancy between the actual and the estimated fibre orientation for increasing values of SNR was assessed in the ROI 1 (cross-area) and ROIs 2, 3 and 4 (parallel-area on side 2). ROIs 2, 3 and 4 correspond to regions with *f* equal to 0.45, 0.57 and 0.65, respectively. $\alpha_1$ and $\alpha_2$ in figure 2 schematically represent the angular difference between the direction of the underlying fibre population (red and blue lines) and estimated direction by means of the maxima of the FOD (a) and the ODF (b) in the cross area (dashed lines). In the case of parallel fibres this discrepancy is quantified by β.

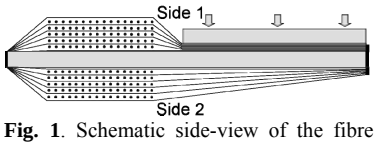


**Fig. 1**. Schematic side-view of the fibre phantom.

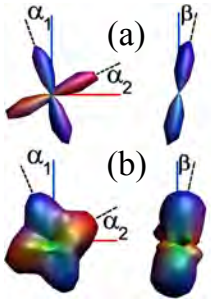


**Fig. 2.** Schematic representation of the deviation angles between the actual (blue and red lines) and the estimated (dashed lines) fibre direction by means of the FOD (a) and the ODF (b). $\alpha_1$ and $\alpha_2$ correspond to the cross-area while β corresponds to the parallel-area.

## Results and discussions

Figures 3a and b demonstrate the FOD and ODF reconstruction, respectively, for increasing values of SNR in the cross-area. Different values of SNR were obtained by increasing the number of averages (1, 2, 4, 8 and 16). They show that uncertainties in evaluation of crossing fibre orientations by both CSD and QBI analysis are rather high for low SNR values (first three columns from the left) but improve as the SNR becomes high enough. This can be seen in figures 3c and d where the dependence of $\alpha_1$ and $\alpha_2$ on SNR is shown. Figures 4a and b show the FOD and ODF, respectively, in the parallel-area of side 2 for different values of SNR and *f*. The first, second, and the third rows in figure 4a and b, correspond to the ROI 2 with low (0.45), ROI 3, intermediate (0.57), and ROI 4, high (0.65) *f* values, respectively. Again, one can see that uncertainties in estimated fibre directions reduce with increasing SNR. Figures 4c and d depict the evolution of β for increasing SNR in the three ROIs.

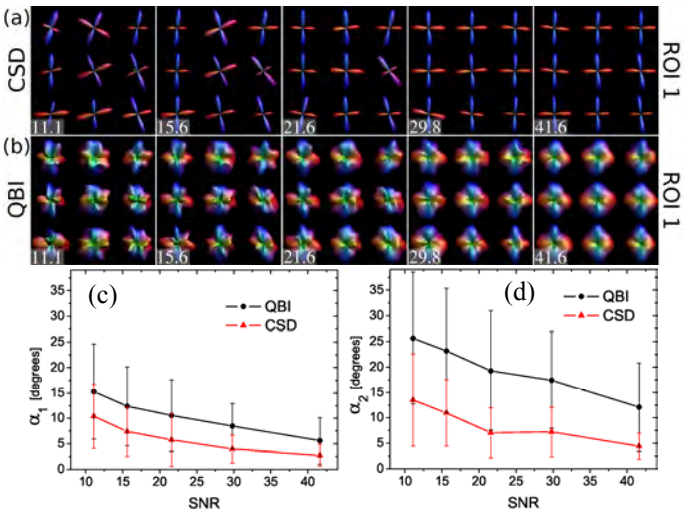


**Fig. 3.** The FOD (a) and ODF (b) in the ROI 1 (cross-area). Dependence of $\alpha_1$ (c) and $\alpha_2$ (d) on SNR. Numbers in the left-bottom are the SNR values

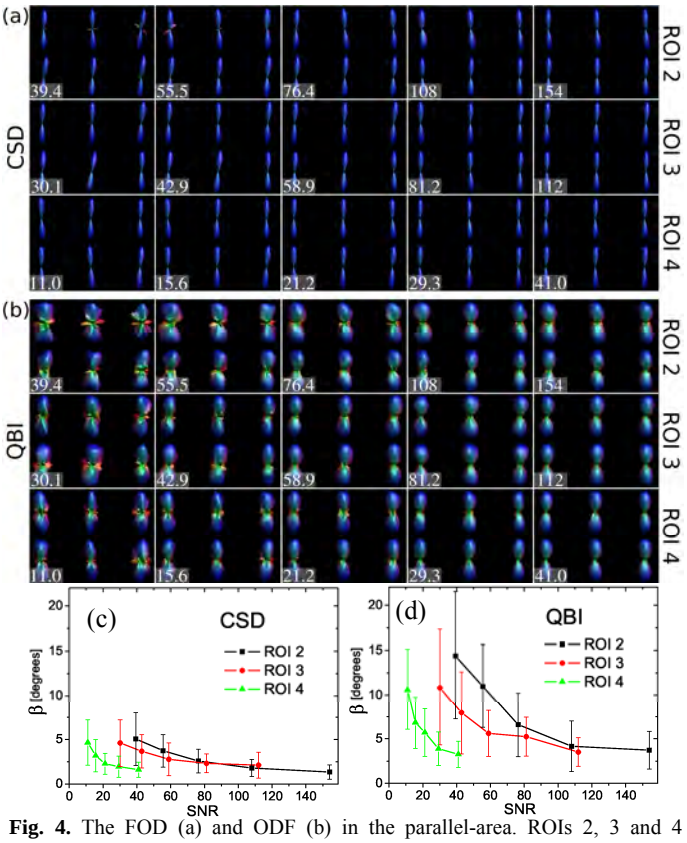


**Fig. 4.** The FOD (a) and ODF (b) in the parallel-area. ROIs 2, 3 and 4 correspond to fibre densities *f* equal to 0.45, 0.57 and 0.65, respectively. Dependence of β for the three ROIs in the case of CSD (c) and QBI (d). Numbers in the left-bottom are the SNR values.

## Conclusions

The applicability of the phantom in HARDI data analysis under clinical conditions was demonstrated. The influence of SNR and fibre density in the estimation of the underlying fibre direction, by means CSD and QBI, was assessed. Both approaches show multi-modal diffusion profiles in the ROI 1 (cross-area) and single-modal diffusion profiles in the ROIs 2, 3 and 4 (parallel-area, side 2).

## References

[1] Farrher, E., Kaffanke, J., Celik, A., Stoecker, T., Grinberg, F., and Shah, N.J. *Magn. Reson. Imaging*, in revision. [2] Tuch, D.S. *Magn. Reson. Med.* **52**, 1358-1372 (2004). [3] Torunier, J.-D., Calamante, F. Connelly, A. *Neuroimage* **35**, 1459-1472 (2007). [4] Leemans, A., Jeurissen, B., Sijbers, J., Jones, D.K. *Proc. Intl. Soc. Mag. Reson. Med.* **17**, 3537 (2009).